IJRSET NOVEMBER 2016 Volume 3, Issue 11 Pages: 35-43

ISSN 2394-739X

International Journal for Research in Science Engineering and Technology

OPTIMIZED MODEL OF ANN USING COAC FOR LLC RESONANT PSFB DC-DC CONVERTER

[1] K. RAMAPRIYA, [2] J. SHANMUGAPRIYA.,M.E,R.. [3] Nitya.,M.E,
[1]PG Scholar, [2, 3] Asst. Professer,
[1, 2, 3] Department of Electrical and Electronics Engineering,

ABSTRACT: An LLC resonant circuit-based (Phase shifted full-bridge) PSFB dc-dc converter with an LC anti-resonant tank for improving the performance of pulse-frequency-modulation (PFM) is proposed with a new Hybrid controller (Continuous orthogonal ant colony (COAC) and (Artificial Neural Network) ANN). The resonant dc-dc converter, named as LLC-LC converter can extend a voltage regulation area below the unity gain with a smaller frequency variation of PFM by the effect of the anti-resonant tank. This advantageous property contributes for protecting over-current in the case of the short-circuit load condition as well as the start-up interval in the designed band of switching frequency. The response time and accuracy is improved in the proposed system by implementing the hybrid system. The efficiency of the proposed system and the response is verified by simulating using MATLAB Simulink.

Keywords: [LLC-LC resonant converter, COAC, ANN, Zero Voltage Switching (ZVS).]

1. INTRODUCTION

An asymmetrical half-bridge LLC resonant dc-dc converter has been gaining the popularity in a variety of switching power supplies encompassing from a small power ICT equipment, LED lighting, battery chargers for electric vehicles, to a dc micro-grid power distribution system due to a soft-switching operation over the wide range of load power; zero voltage soft-switching (ZVS) of active switches. The wide range of soft switching operation in the LLC converter is attractive for a full-bridge dc-dc converter topology as well, while a typical phase-shift pulse-width-modulation (PS-PWM) full bridge circuit topology suffers from a severely-limited range of soft switching for load power variations. This paper presents the performance of the LLC-LC resonant converter with the complete simulation results on soft switching performance, output voltage and power regulations, power conversion efficiency and loss analysis, including the design consideration of resonant tank parameters, all of which are not mentioned or evaluated in any past reference papers. On comparing to the conventional system the feasibility and efficiency of the LLC-LC resonant topology are proven. The response time and the accuracy in the proposed system is much improved on proposing the system with hybrid controlling technique (COAC and ANN).

2. RELATED WORKS

F. Musavi, M. Craciun, D.S. Gautuam,W. Eberle, andW.G. Dunford, they presented a high performance LLC multi resonant dc–dc converter in a two-stage smart battery charger for neighborhood electric

vehicle applications. The multi resonant converter has been analyzed and its performance characteristics were presented. It eliminated both low- and high frequency current ripple on the battery, thus maximizing battery life without penalizing the volume of the charger. The wide range of soft switching operation in the LLC converter is attractive for a full-bridge dc-dc converter topology as well, while a typical phase-shift pulse-width-modulation (PS-PWM) full bridge circuit topology suffers from a severely-limited range of soft switching for load power variations. [1] W. Feng and F.C. Lee, A soft start-up process for the LLC resonant converter was investigated and optimized based on a graphical state-trajectory analysis. By setting a limitation band at the time proposing, several optimal switching patterns are proposed to settle the initial condition. After that, by sensing the output voltage, the optimal switching frequency was determined within the current limiting band. That virtually guaranteed that there won't be any current and voltage stress in the resonant tank during the soft start-up process. Meanwhile, the output voltage was built up quickly and smoothly. Although it can be effective for the start-up process, no over current protection is guaranteed for the short-circuit load condition by the hybrid pulse modulation scheme. This technical problem will affect on feasibility and reliability of power converters in the dc-source power supplies such as microgrid and transportation applications. [2] X. Xie, J. Zhang, C. Zhao, Z. Zhao, and Z. Qian, A novel over-current protection method for LLC resonant converter was presented by them. This method was very attractive for its good current limit ability, especially under short circuit condition. Moreover, its current limit point range was easy to be optimized. This technique is, however, effective only for a low output voltage application since the clamping voltage depends on the output voltage, accordingly not suitable for the full-bridge topology. In addition, the auxiliary transformer and rectifier diodes will lead to increase of power losses and deteriorate the efficiency under light load conditions. [3] D. Fu, F.C. Lee, Y. Liu, and M. Xu, A novel multi-element resonant converter for front-end dc/dc converters was proposed. The superior performance of the proposed resonant converters was to provide inherent current protection and very low circulating energy. With the optimized design, the proposed resonant converters can operate under short output circuit. Based on the third order harmonic injection, the circulating energy of the resonant tank was reduced and lower than other conventional resonant converters, such as LLC resonant converters. Zero-voltage-switching (ZVS) and Zero-current-switching (ZCS) were achieved for primary side and secondary side devices respectively. However, the main argument of the literature is focused on exploring a method of magnetic integration of resonant inductors and utilizing the third harmonics components. Injection of the harmonics components will lead to decrease of the most useful component; fundamental frequency (switching frequency) active power, consequently the converter efficiency might deteriorate especially for the full-bridge LLC converter applications. [4] H. Mizutani, T. Mishima, and M. Nakaoka, The LLC DC–DC converter proposed here in can improve the sensitivity of voltage conversion ratio in the step-down area, and then achieve the excellent performance on the output voltage and power regulations by pulse frequency modulation (PFM) under soft switching conditions. The theoretical analysis and the experiment results on the essential switching and steady-state performances of the proposed DC–DC converter effectiveness were verified. The original idea of the proposed resonant converter is to achieve Over-Current Protection (OCP) with a designed anti-resonant frequency and characteristics impedance while the operating principle of the LLC converter is retained under the normal load condition between two series resonant frequencies. Where on high frequencies the harmonic components are includes. [5]

3. PROPOSED SYSTEM

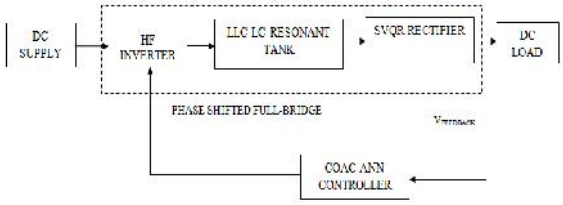

Figure 1- Block diagram of proposed system

The proposed system block diagram is shown in the Fig.1. We have used hybrid controller (COAC-ANN) techniques to improve the efficiency and accuracy in the system.

4. LLC-LC RESONANT DC–DC CONVERTER

Circuit Topology and Operating Principle:

The LLC-LC resonant full-bridge dc-dc converter is schematically depicted in Fig. 2. The anti-resonant tank (Lp-Cp) is employed in series with the series resonant network (Ls-Cs) in the primary-side HF inverter.

$$f_{r1} = \sqrt{\frac{f_{rs}^2 + \lambda_{rs}^{-1} f_{rs} f_{rp} + f_{rp}^2 - \sqrt{\left(f_{rs}^2 + \lambda_{rs}^{-1} f_{rs} f_{rp} + f_{rp}^2\right)^2 - 4 f_{rs}^2 f_{rp}^2}}{2}}$$

$$f_{r2} = \sqrt{\frac{f_{rm}^2 + \lambda_{rm}^{-1} f_{rm} f_{rp} + f_{rp}^2 - \sqrt{\left(f_{rm}^2 + \lambda_{rm}^{-1} f_{rm} f_{rp} + f_{rp}^2\right)^2 - 4 f_{rm}^2 f_{rp}^2}}{2}} \quad \text{-- (1)}$$

The converter has two series resonant frequencies; the first resonant frequency fr1 and the second resonant frequency fr2, where Qrp (= Zrp/Rac) denotes the impedances ratio with respect to the anti-resonant tank. The series and anti-resonant tank impedances Zs, Zp are defined respectively as

$$Z_s = \left|\dot{Z}_s\right| = \left|j\left(\omega_s L_s - \frac{1}{\omega_s C_s}\right)\right|$$

$$Z_p = \left|\dot{Z}_p\right| = \left|\frac{j\omega_s L_p}{1 - \omega_s^2 L_p C_p}\right|. \quad \text{---- (2)}$$

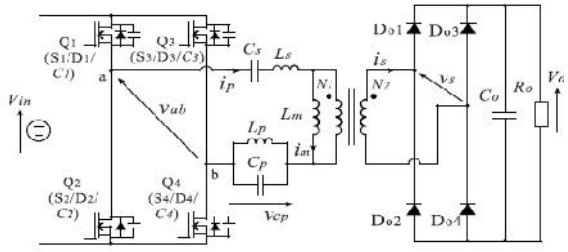

Figure2- LLC-LC resonant full-bridge dc-dc converter

Based on the above equations, the typical characteristics of series and anti-resonant tank impedances versus switching frequency are illustrated in Fig.3. According to the PFM scheme, Zs and Zp are correlatively expressed as

$$\begin{aligned} &f_{r2} \le f_s < f_{r1} \Rightarrow Z_s \gg Z_p \\ &f_s = f_{r1} \Rightarrow Z_s = Z_p \\ &f_{r1} < f_s < f_{rp} \Rightarrow Z_s < Z_p \\ &f_s = f_{rp} \Rightarrow Z_p \to \infty. \end{aligned} \quad \text{--- (3)}$$

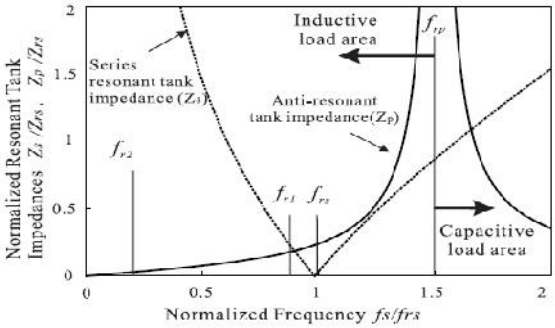

Figure 3- Theoretical characteristics of the series and anti-resonant impedances versus switching frequency in the LLC-LC converter

The HF transformer primary-side current I^*_p under the short-circuit and overload conditions can be theoretically expressed at fs = frp as

$$I_p^* = \frac{V_{rp,max}}{Z_p} = \frac{4V_{in}(1 - \omega_s^2 L_p C_p)}{\pi \omega_s L_p} \to 0 \quad \text{--- (4)}$$

The frequency-domain equivalent circuits of the proposed LLC-LC converter are illustrated in Fig. 4, where the frequency-dependent modifications are included in accordance with (8)-(11). The input impedance Zin' can be defined on the basis of Fig. 7

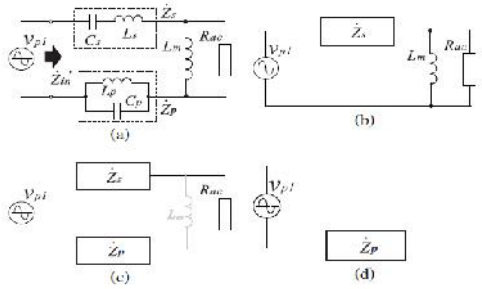

Figure 4-Simplified equivalent circuits of LLC-LC converter: (a) common topology, and modified for (b) fr2 ≤ fs < fr1, (c) fr1 ≤ fs < frp, (d) fs = frp.

$$Z_{in}' = \left|Z_{in}'\right| = \left| \frac{\omega_s L_m \left[1-(1-F_{rs}^{2})F_{rs}^{-2}-(1+1/\gamma_1)F_{rs}^{-2}\right]}{\omega_s C_r \left[1-F_{rs}^{-2}\right]\left[R_{ac}+j\omega_s L_m\right]} - j\frac{R_{ac}\left[1-(1-F_{rp}^{-2})F_{rp}^{-2}-(1-\gamma_1)F_{rp}^{-2}\right]}{\omega_s C_r \left[1-F_{rp}^{-2}\right]\left[R_{ac}+j\omega_s L_m\right]} \right| \quad \text{- (5)}$$

Based on above equation, the input impedance versus switching frequency curves are depicted in Fig. 5. In fr2 ≤ fs ≤ fr1; ZVS area 1, Zin' exhibits the property similar to Zin, thus no significant difference on the operating characteristics appears between the LLC and LLC-LC converters. On the other hand, Zin' escalates with a high sensitivity in fr1 < fs ≤ frp; ZVS area 2. In order to mitigate the influence of anti-resonant tank in the ZVS area 1, the input impedance of the LLC-LC converter should be designed as compatible with the LLC converter.

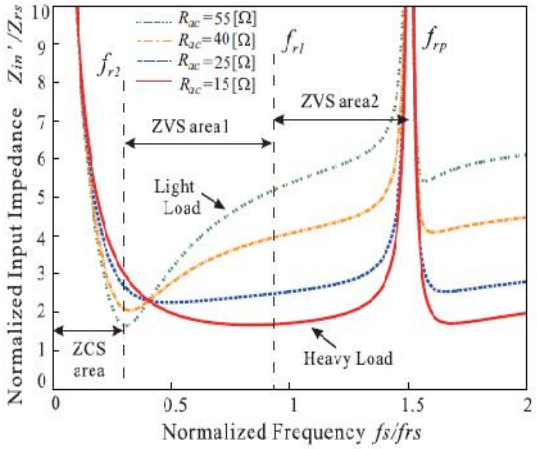

Figure 5- Theoretical input impedance characteristics of LLC-LC converter

$$M = \frac{1}{\alpha\sqrt{\left(1+\frac{\xi}{\omega_s L_m}\right)^2 + \left[Q_{rs}\left(F_{rs}-\frac{1}{F_{rs}}\right) - Q_{rp}\left(F_{rp}-\frac{1}{F_{rp}}\right)^{-1}\right]^2}} \quad \text{-- (5)}$$

$$\xi = Z_{rs}\left(F_{rs}-\frac{1}{F_{rs}}\right) - Z_{rp}\left(F_{rp}-\frac{1}{F_{rp}}\right)^{-1} \quad \text{-- (6)}$$

The theoretical voltage conversion ratio M of the proposed converter can be derived similarly from FHA as equation above. Based on M, the theoretical curves of the voltage conversion ratio and output power versus the normalized switching frequency are shown in Fig.6. Those curves indicate the dc voltage conversion ratio decreases due to the highsensitivity of PFM in the ZVS area 2, consequently the output voltage can be regulated over the wide range of load power variations by the effect of the anti-resonant tank. It should be remarked the FHA-based analysis is effective for the proposed converter since the harmonics in the resonant currents of the primary- and secondary-side circuits can be suppressed by designing frp and Zrp.

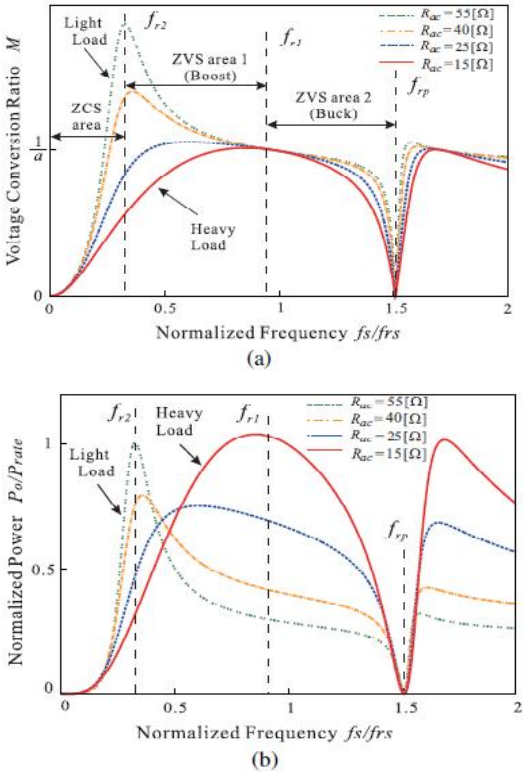

Figure 6- Theoretical characteristics of the LLC-LC converter: (a) M– normalized fs, and (b) normalized Po–normalized fs.

5. SWITCHING MODE TRANSITIONS

The key operating waveforms and mode-transition equivalent circuits of the proposed converter for the ZVS area 1 (boost voltage regulation) are shown in Figs.7 (a) and (b), respectively. The circuit operation during one switching cycle can be divided into ten modes as follows:

Mode 1 [power transfer mode (im reverses its polarity and linearly increases): t0 ≤ t < t1] The polarity of the magnetizing current im reverses from negative to positive at t = t0. During this interval, the active switchesQ1 and Q4 are on-state, then the power starts to be fed from the input voltage source Vin to the load Ro. The primary-side HF inverter current ip gradually decays toward zero by the effect of series resonance. **Mode 2** [Do1, Do4

ZCS turn-off mode: t1 ≤ t < t2] The primary-side current ip decreases gradually due to the series resonance by Ls and Cs, then it corresponds to im at t = t1. The secondary-side current is naturally becomes zero, as a result Do1 and Do4 can be turned off by ZCS with a minimized reverse recovery current. During this interval, im appears only in the primary-side HF inverter, while the secondary-side rectifier gets into the discontinuous conduction current mode (DCM). **Mode 3** [Q1, Q4 ZVS turn-off mode: t2 ≤ t < t3] The gate signals for Q1 and Q4 are removed at t = t2. Then, their voltages vQ1 and vQ4 rise gradually from zero with the effects of parasitic, or the lossless snubber capacitors C1–C4, while the voltages vQ2 and vQ3 across Q2 and Q3 decrease gradually from Vin to zero. ZVS turn-off herein can be attained by im in Q1 and Q4. During this interval, ZVS condition is defined by

$$\frac{1}{2}L_m i_m(t_2)^2 > 2C_r V_{in}^2, \quad \text{--- (7)}$$

Where Cr represents the lossless snubber capacitor C1 = C2 = C3 = C4.

Mode 4 [Q2,Q3 ZVS&ZCS turn-on /Do2,Do3 ZCS turn-on mode: t3 ≤ t < t4] The voltages vQ2 and vQ3 across Q2 and Q3 reach to zero at t = t3 due to the edgeresonance sustaining from Mode 3, there by D2 and D3 are forward-biased. During this interval, the gate terminals of Q2 and Q3 are triggered, thereby ZVS&ZCS turn-on commutation can be achieved in the two switches. At the same time, ip reverses its polarity, then is begins to rise gradually from zero. Thus, ZCS turn-on can be obtained in Do2 and Do3.

Mode 5 [power transfer mode (im linearly decreases): t4 ≤ t < t5] At t = t4, the current through Q2 and Q3 commutate from D2 and D3 to S2 and S3. Accordingly, power transfers from Vin to Ro in the resonant behavior.

Mode 6 [power transfer mode (im reverses its polarity and linearly decreases): t5 ≤ t < t6] The polarity of im reverses from positive to negative at t = t5. During this interval, Q2 and Q3 are on-state, then power starts to be fed from Vin to Ro. Accordingly, ip gradually decays toward zero by the effect of series resonance.

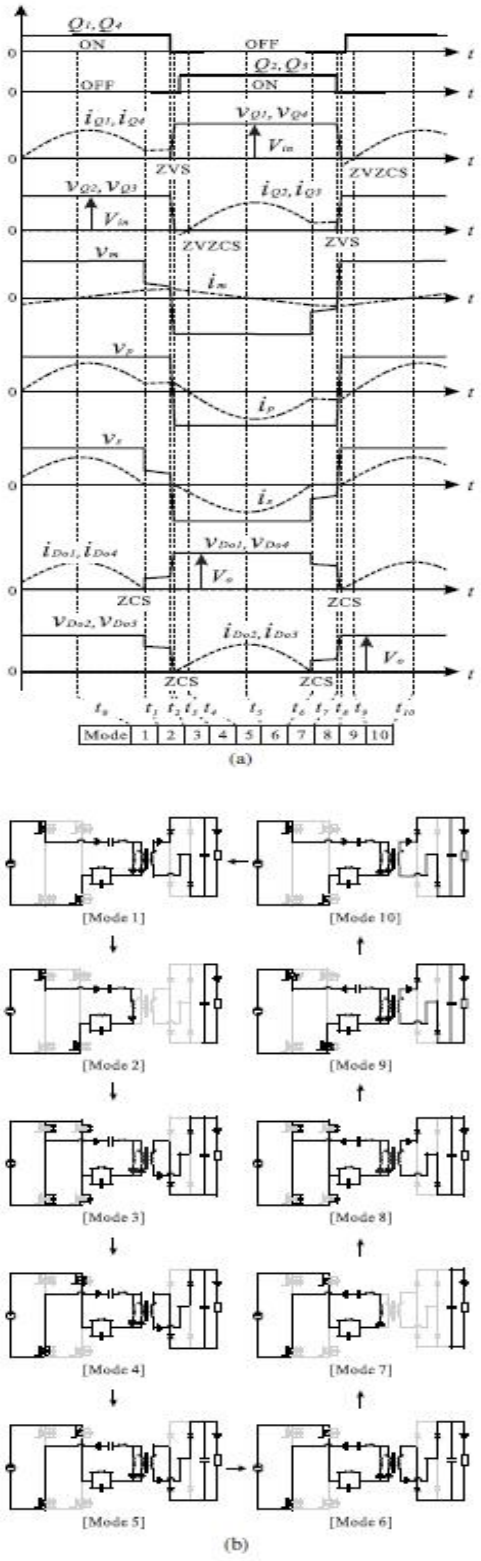

Figure7- Key voltage and current waveforms, and switch-mode transitions operating in fr2 ≤ fs ≤ fr1 (ZVS area 1): (a) voltage and current waveforms during one switching-cycle, and (b) equivalent circuits

Mode 7 [Do2,Do3 ZCS turn-off mode: t6 ≤ t < t7] The primary-side ip decreases gradually due to the series resonance by Ls and Cs, and it corresponds with im at t = t6. Then, the secondary-side is naturally becomes zero, as a result Do2 and Do3 can be turned-off by ZCS with a minimized reverse recovery current. During this interval, im appears only in the primary-side circuit, while the secondary-side power stage gets into DCM.

Mode 8 [Q2,Q3 ZVS turn-off mode: t7 ≤ t < t8] The gate signals for Q2 and Q3 are removed at t = t7. Then, their voltages vQ2 and vQ3 rise gradually from zero with the effects of parasitic, or the lossless snubber capacitors C1 − C4, while the voltages across Q1 and Q4 decrease gradually from Vin to zero. ZVS turn-off herein can be attained by im in Q2 and Q3. During this interval, ZVS condition is expressed by

$$\frac{1}{2}L_m i_m(t_7)^2 > 2C_r V_{in}^2. \quad \text{------ (8)}$$

Mode 9 [Q1,Q4 ZVS &ZCS turn-on /Do1,Do4 ZCS turn-on mode: t8 ≤ t < t9]

The terminal voltages vQ1 and vQ4 reach to zero at t = t8 due to the edge resonance sustaining from Mode 8, then D1 and D4 are forward-biased. During this interval, the gate terminals of Q1 and Q4 are triggered, thereby ZVS&ZCS turn-on commutation can be achieved in those switches. At the same time, ip reverses its polarity, then is begins to rise gradually from zero. Thus, ZCS turn-on can be obtained in Do1 and Do4.

• Mode 10 [power transfer mode (im linearly increases): t9 ≤ t < t10]

At t = t9, the current through Q1 and Q4 commutate from D1 and D4 to S1 and S4. Accordingly, the power transfer stars from Vin to Ro in the resonant behavior.

The voltage and current waveforms for the ZVS area 2 (buck voltage regulation) are depicted in Fig.7 (a), and the corresponding circuit transitions are illustrated in Fig. 7 (b), respectively. The secondary-side current is is naturally continuous in the ZVS area 2, so the operating and commutation process is similar to ZVS area 1 with the exception of Mode 2 and Mode 7 mentioned above.

The time-domain formulas with high-order differential equations are summarized in TABLE I for the ZVS area 1 and the ZVS area 2, respectively. The resonant capacitor voltage vcs of the series resonant tank is selected as the state valuable to express the steady-state operations of the proposed coverer. Accordingly, the current iLs through Ls, current iLp through Lp and voltage vcp across Cp can be expressed on the basis of vcs as

$$i_{Ls} = C_s\frac{dv_{cs}}{dt},\ i_{Lp} = \frac{-\omega_s^2 L_p C_p i_{Ls}}{1-\omega_s^2 L_p C_p},\ v_{cp} = L_p\frac{di_{Lp}}{dt}. \quad \text{------- (9)}$$

6. IMPLEMENTATION OF COAC

The main steps in continuous orthogonal ant colony (COAC) algorithm are the orthogonal exploration and the global modulation. An overall flowchart of COAC is illustrated in Fig.8, where MAXITER is the predefined maximum number of the iteration number. A complete set of pseudo code of the COAC algorithm for a minimization problem is below.

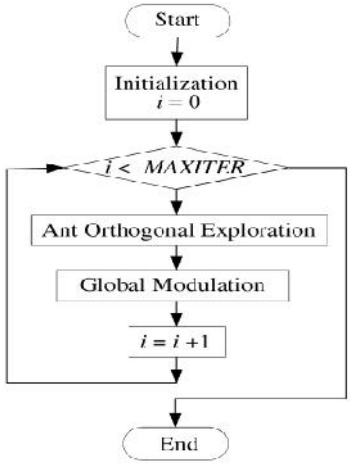

Figure 8- Flowchart of the continuous orthogonal ant colony (COAC)

7. ARTIFICIAL NEURAL NETWORK (ANN)

An Artificial Neural Network (ANN) can be defined as the information processing paradigm, which is inspired by the human biological nervous system. It is composed of a large number of highly interconnected processing elements known as neurons to

solve computational problems. An important criterion of ANN is the ability of learning from the environment. Synaptic or weight connections that exist between the neurons in the nervous system are adjusted in order to learn. ANN consists of a number of artificial neurons which receive a number of inputs. A function called activation or cost function is applied to these inputs resultant in an activation level of a neuron. Knowledge about the learning task is given in the form of examples called training examples. ANN is defined by architecture, neuron model and the learning algorithm. Architecture refers to a set of neurons and links connecting neurons with weights. Neuron model refers to the information-processing unit of the ANN.

8. THE WORKING OF ARTIFICIAL NEURAL NETWORKS

Certainly, ANN can often provide a suitable solution for problems that are generally characterized by nonlinear, high dimensionality, noisy, complex, imprecise, imperfect and/or error-prone sensor data, poorly understood physical and statistical models, and lack of clearly stated mathematical solution or algorithm. Mostly ANN approaches are capable of solving scientific, electrical engineering, earth knowledge, mathematical and of course statistical tasks. The determination of the network architecture is one of the most important steps in developing a model for a given problem. Although ANN construction has been extensively investigated by various researchers, there is no known procedure or algorithm for this process for the general case. Two approaches have been proposed, namely constructive and destructive methods. In both constructive and destructive methods, the numbers of hidden nodes are considered. The fundamental composition block of every ANN is the artificial neuron. That is, a simple mathematical functions or model combination such as multiplication, summation and activation. At the doorway of an artificial neuron, the input signals are weighted, implying that every input value is multiplied by individual weight values. The center distribution of an artificial neuron is addition function that sums all weighted values, input signals and bias values. The final step or output layer of an artificial neuron is the sum of earlier weight values; input signals and bias are passing through transfer function also called activation function for getting target values. There are different activation or transfer function uses for getting the best target which depends on the output and behaviors of the data. Fig.9 shows the universal ANN structure.

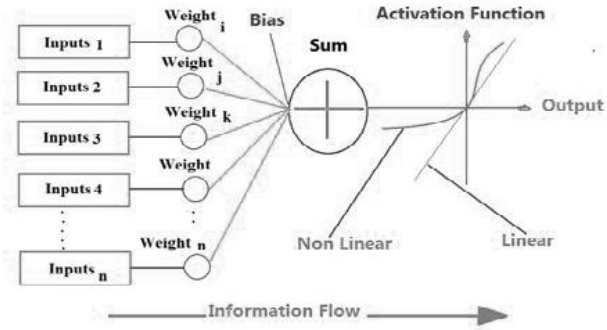

Figure 9-Artificial neuron working model

Each input has an associated weight w, which can be modified in order to model synaptic learning. The unit computes some function f of the weighted sum of its inputs by equation below:

$$y_i = f_i\left(\sum_{i=1}^{n} w_i x_i + bias\right)$$

-------- (10)

9. PROPOSED SIMULATION MODULE

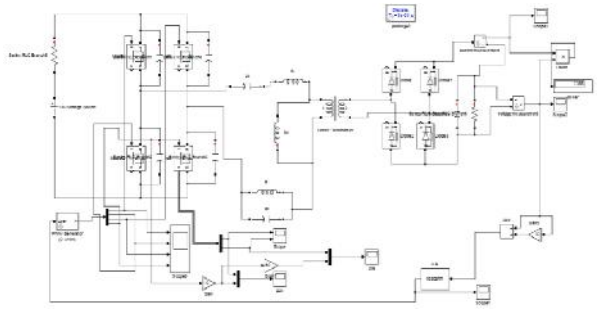

Figure 10- Simulation Module of Proposed System

The simulation module of the proposed system is shown above. Here we have DC

source supply and phase shifted full bridge converter including LLC-LC circuit. We have proposed the existing system by implementing hybrid system. In hybrid system we have used COAC and ANN controlling technique.

10. SIMULATION RESULTS

The simulation module is designed using MATLAB Simulink and the output results are verified. The simulation result waveforms are shown below.

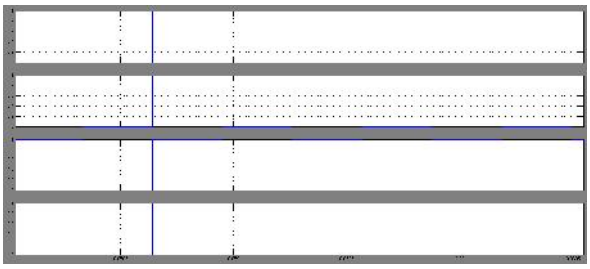

Figure 11-Switching pulse for High frequency (HF) inverter

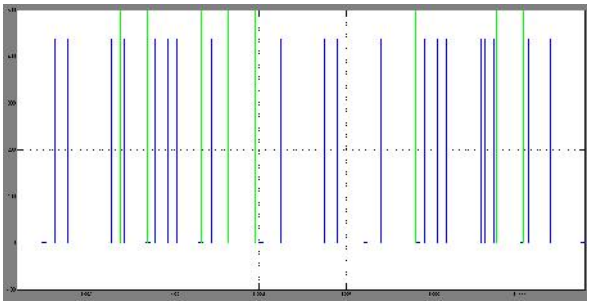

Figure 12- Zero Voltage Switching (ZVS)

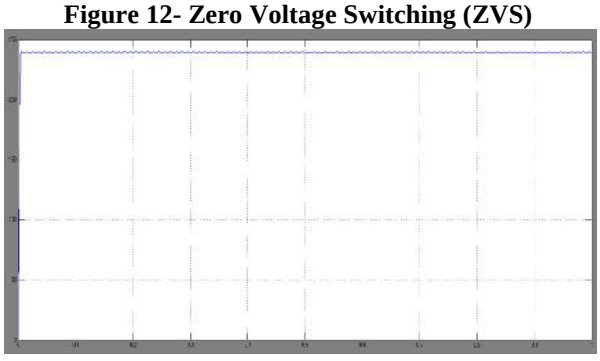

Figure 13- Output DC voltage waveform

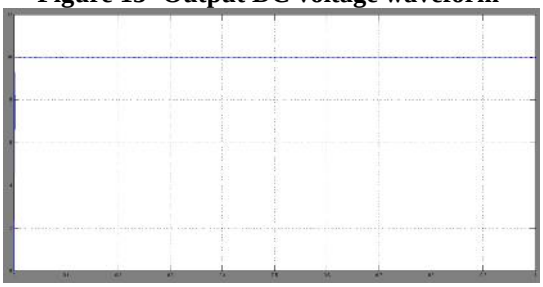

Figure 14-Output DC current waveform

CONCLUSION

This paper presents an LLC resonant circuit-based (Phase shifted full-bridge) PSFB dc-dc converter with an LC anti-resonant tank for improving the performance of pulse-frequency-modulation (PFM) with a new Hybrid controller Continuous orthogonal ant colony (COAC) - (Artificial Neural Network) ANN). The over-current protection for the short-circuit load condition as well as a start-up interval can be ensured in a smaller band of switching frequency which is designed on the basis of the series and anti-resonant frequencies. The voltage regulation is good in the proposed system. The proposed system is simulated using the MATLAB Simulink and the output is verified.

REFERENCE

[1]. F. Musavi, M. Craciun, D.S. Gautuam,W. Eberle, andW.G. Dunford, ”An LLC resonant dc-dc converter for wide output voltage range battery charging applications,” IEEE Trans. Power Electron., vol.28, no.12, pp.5437–5455, Dec. 2013.

[2]. W. Feng and F.C. Lee, ”Optimal trajectory control of LLC resonant converters for soft start-up,” IEEE Trans. Power Electron., vol.29, no.3, pp.1461–1468, Mar. 2014.

[3]. X. Xie, J. Zhang, C. Zhao, Z. Zhao, and Z. Qian, “Analysis and Optimization of LLC resonant converter with a novel over-current protection circuit,” IEEE Trans. Power Electron., vol.22, no.2, pp.435–443, Mar. 2007.

[4]. D. Fu, F.C. Lee, Y. Liu, and M. Xu, “Novel multi-element resonant converter for front-end dc-dc converters”, in Proc. IEEE Power Electron. Special., Conf. (PESC), Jun. 2008, pp.250– 56.

[5]. H. Mizutani, T. Mishima, and M. Nakaoka, “A novel LLC multiresonant dc-dc converter with an anti-resonant circuit”, in Proc. 7th Int. Power Electron. Motion Control Conf. (IPEMC), Jun. 2012, pp.1324- 1335.

[6]. T. Jiang, J. Zhang, X.Wu, K. Sheng, and Y.Wang, ”Bidirectional LLC resonant converter with automatic forward and

backward mode transition," IEEE Trans. Power Electron., vol.30, no.2, pp.757–770, Feb. 2015.
[7]. H. Mizutani, T. Mishima, and M. Nakaoka, "A dual pulse modulated fiveelement multi-resonant dc-dc converter and its performance evaluations", in Proc. IEEE Energy Convers. Congr. Expo. (ECCE), Sep. 2013, pp.4912–4919.
[8]. Z. Liang, R.Guo, L. Li, and A.Q. Huang, "A high-efficiency PV moduleintegrated dc-dc converter for PV energy harvest in FREEDM system," IEEE Trans. Power Electron., vol.26, no.3, pp.897–909, Mar. 2011.
[9]. J. Zhang, J.Wang, G. Zhang, and Z. Qian, "A hybrid driving scheme for full-bridge synchronous rectifier in LLC resonant converter," IEEE Trans. Power Electron., vol.27, no.11, pp.4549–4561, Nov. 2011.
[10]. H. Hu, X. Fang, F. Chen, Z.J. Shen, and B. Batarseh, "A modified highfrequency LLC converter with two transformers for wide input-voltage range applications", IEEE Trans. Power Electron., vol.28, no.4, pp.1946-1960, Apr. 2013.
[11]. D.Wong, and Y. Liu, "Zero-crossing noise filter for driving synchronous rectifiers of LLC resonant converter," IEEE Trans. Power Electron., vol.29, no.4, pp.1953–1965, Apr. 2014.
[12]. J.-Y. Lee, Y.-S. Feong, and B.-M. Han, "An isolated dc-dc converter using high-frequency unregulated LLC resonant converter for fuel cell applications," IEEE Trans. Ind. Electron., vol.58, no.7, pp.2926-2934, Jul. 2011.
[13]. W. Hong, H.J. Kim, J.-S. Park, Y.-G. Pu, J. Cheon, D.-H. Han, and K.- Y. Lee, "Secondary-side LLC resonant controller IC with dynamic PWM dimming and dual-slope clock generator for LED backlight units," IEEE Trans. Power Electron., vol.26, no.11, pp.3410-3422, Nov. 2011.